White Rose Research Online
eprints@whiterose.ac.uk
https://eprints.whiterose.ac.uk
Universities of Leeds, Sheffield and York

Deposited via The University of Leeds.

White Rose Research Online URL for this paper:
https://eprints.whiterose.ac.uk/id/eprint/224573/

Version: Accepted Version

Article:

Mitrichev, I., Blacker, A.J., Chapman, M. et al. (2025) DFT-Assisted Microkinetic Study of Transfer Hydrogenation over Homogeneous and Immobilized Cp*Ir Complexes. The Journal of Physical Chemistry A, 129 (10). ISSN: 1089-5639

https://doi.org/10.1021/acs.jpca.4c08718

This is an author produced version of an article accepted for publication in The Journal of Physical Chemistry A, made available under the terms of the Creative Commons Attribution License (CC-BY), which permits unrestricted use, distribution and reproduction in any medium, provided the original work is properly cited.

Reuse

This article is distributed under the terms of the Creative Commons Attribution (CC BY) licence. This licence allows you to distribute, remix, tweak, and build upon the work, even commercially, as long as you credit the authors for the original work. More information and the full terms of the licence here: https://creativecommons.org/licenses/

Takedown

If you consider content in White Rose Research Online to be in breach of UK law, please notify us by emailing eprints@whiterose.ac.uk including the URL of the record and the reason for the withdrawal request.

UNIVERSITY OF LEEDS
University of Sheffield
UNIVERSITY of York

DFT-assisted Microkinetic Study of Transfer Hydrogenation over Homogeneous and Immobilized Cp*Ir Complexes

Ivan Mitrichev,[a] A. John Blacker,[b,c] Michael Chapman,[b] Yuji Kawakami,[c][†] Mikhail Vasilev,[a] Gert Goltz,[b] Anna Podobedova,[a] Antonia Borissova,[b] Eleonora Koltsova[a]*

[a] Information Computer Technologies Department
D. Mendeleev University of Chemical Technology of Russia
9, Miusskaya sq., 125047 Moscow (Russia)

[b] Institute of Process Research and Development
School of Chemical and Process Engineering
University of Leeds
Woodhouse Lane, LS2 9JT Leeds (The United Kingdom)

[c] Institute of Process Research and Development
School of Chemistry
University of Leeds
Woodhouse Lane, LS2 9JT Leeds (The United Kingdom)

Keywords. immobilized catalyst, hydrogen transfer, microkinetic modelling, density functional calculations, reaction mechanisms.

Abstract. DFT calculations were done to investigate kinetic mechanism of benzaldehyde transfer hydrogenation using $[Cp^*IrCl_2]_2$ complexes in isopropyl alcohol in the presence of potassium *tert*-butoxide. Predicted energy barriers provide an evidence that the inner sphere mechanism (effective barrier 53.0 kJ/mol) is favoured over the outer sphere and MPV mechanisms.

Reaction kinetics was studied using both homogeneous and immobilized Cp*Ir complexes as catalysts. A mathematical model was developed to simulate the transfer hydrogenation of benzaldehyde on these catalysts, accounting possible mass transfer limitations for the immobilized catalyst. A microkinetic model was constructed both using our density functional theory calculations and fitting the kinetic parameters of catalyst activation and deactivation reactions.

Simulation results predict that only about a quarter of Ir immobilized complexes are involved into reaction, and this is the main reason for the observed higher activity of the homogeneous catalyst. The activity of the immobilized catalyst was found to be related to the hydride species concentration, which is a function of base concentration. The results suggest that the amount of base has a drastic effect on immobilized catalyst activity.

Introduction

Catalytic transfer hydrogenation uses solution phase donor molecules as hydrogen sources rather than gaseous hydrogen. This simplifies the process, is non-hazardous,[1] and although it produces a by-product it allows the use of cheap sources such as *iso*-propanol and formic acid. The catalytic reaction is applied in the reduction of C=O and C=N bonds to obtain alcohols and amines and is of great importance for the pharmaceutical, food and agrochemical industries.[2] A lot of studies are devoted to asymmetric transfer hydrogenation, which allows the production of chiral alcohols.[3–5] Homogenous Ir-, Ru- and Rh-containing complexes with effective ligands are effective transfer hydrogenation catalysts.[6,7] However, in industry supported catalysts are preferred because they can be easily separated from the reaction mixture and recycled. Furthermore, they provide a fixed-bed over which reactions can be continuously flowed. Blacker and co-workers reported a strategy for immobilization of group 9 catalysts *via* a strong η^5-coordinated penta-alkylcyclopentadienyl (Cp*) ligand which prevents metal leaching that is a problem when traditional mono- or bi-dentate ligands are used.[8] The $[Cp^*IrCl_2]_2$ complex **1** is known to be active in hydrogen transfer reactions, and its hydroxyl tethered counterpart **2** can be immobilized on a Wang resin support to give the immobilized catalyst **3** (Scheme 1). The catalyst **3** is active in transfer hydrogenation and can be used up to 30 times in batch, or used in continuous flow with lifetimes of 120 hours.[8,9]

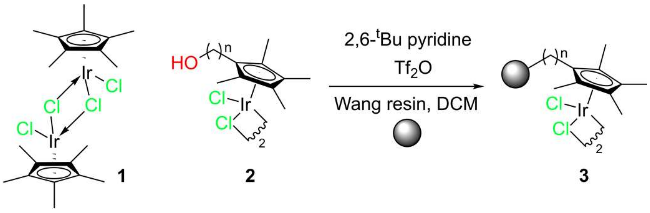

Scheme 1. The homogeneous (**1**), hydroxyl tethered (**2**) and immobilized (**3**) $[Cp^*IrCl_2]_2$ catalysts.

It is well known that reactions on immobilized catalysts have low rates compared with homogeneous catalysts, and this is also the case with IrCp* catalysts.[8–10] This may be due to differences in kinetics, number of active species or due to the presence of mass transfer limitations for the immobilized catalyst. The lack of explanation of the observed differences hampers process optimization and scale-up.

Microkinetic modelling has proven to be a powerful tool in heterogeneous catalysis studies, yet is rarely applied in homogeneous catalysis.[11,12] Single studies employ it in the area of liquid phase catalysis.[13,14] Nevertheless, it can be useful to relate observed features, such as catalytic activity and deactivation, to key intermediates and rate-limiting steps. The combination of a suitable flow and mass transfer models with a microkinetic model can be used to simulate reactions both on homogeneous and on immobilized catalysts. Since the model is based on detailed reaction kinetics, it should include the main reaction pathways.[15]

The transfer hydrogenation of ketones usually proceeds through metal hydride intermediates,[16–18] that include inner sphere (IS) and outer sphere (OS) mechanisms. In the IS mechanism, the substrate coordinates to the metal prior to hydride transfer (Scheme 2a). This mechanism was found preferable for [Ir(μ-OMe)(diolefin)]$_2$ complexes with P- and N- donor ligands,[19] as well as for Ir complexes with chelating bis(NHC) ligands.[20] In the OS mechanism, the substrate does not coordinate to the metal site, but remains in the outer coordination sphere (Scheme 2b).[16] The classical OS hydrogenation mechanism relies on the concept of metal-ligand bifunctional catalysis with involvement of a ligand.[21] A proton is transferred to the substrate using the X-H unit (X=N, O) of the ligand and the hydride is transferred from the metal.[21]

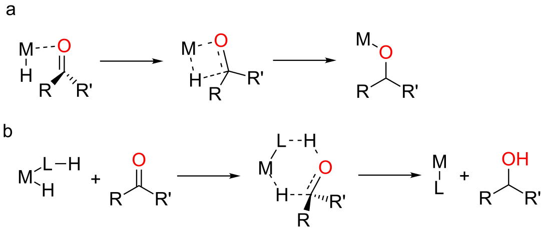

Scheme 2. (a) Inner sphere and (b) outer sphere transfer hydrogenation.

Some studies show that monohydride pathways are not unique,[22,23] or can even be disfavoured with respect to the Meerwein–Pondorf–Verley mechanism (MPV),[24] in which both reactants coordinate to the metal site prior to the direct hydride transfer between them.

The aim of this work is to create a microkinetic model based on density functional theory (DFT) calculations, which explain the differences in transfer hydrogenation rate using homogeneous chloride complex **1** and the immobilized chloride complex **3**. For simplicity, we have chosen benzaldehyde as a substrate, and *iso*-propanol as both hydrogen donor and solvent.

The study was organised as follows: first, a DFT mechanistic study of IS, OS and MPV mechanisms with experimental kinetics; then, a DFT-assisted microkinetic model was constructed and the missing kinetic (catalyst activation and deactivation) and mass-transfer parameters were fitted using experimental benzaldehyde conversion values. The simulation employs a mathematical model that allows transfer hydrogenation simulation using both homogeneous and immobilized catalysts. Conclusions were drawn on the reaction mechanism and on the reasons for differences in transfer hydrogenation rate for **1** and **3**. The results of additional studies on the model are discussed.

Computational method

DFT calculations on the three mechanisms (IS, OS, MPV) for the homogeneous catalyst **1** with benzaldehyde were carried out using Orca 5.0.3 software.[25] Triple-zeta polarized basis sets def2-TZVP were employed for all atoms except Ir.[26,27] For iridium, ECP60MWB effective core potential (ECP) with the associated triple-zeta quality valence basis set was used.[27,28] The RI-J approximation for Coulomb integrals with the corresponding auxiliary basis set (def2/J)[29] and COSX integration for Hartree-Fock (HF) exchange implemented in Orca were employed to speed-up the calculations.

Geometry optimization and vibrational frequency analysis were done using B3LYP-D3(BJ) exchange-correlation hybrid functional.[30,31,32] The climbing image nudged elastic band (CI-NEB) method following the transition state optimization (NEB-TS) was used to find transition states.[33,34]

Each transition state had only one imaginary frequency. DSD-BLYP-D3(BJ)[35] double hybrid functional, which is more accurate than B3LYP-D3(BJ) in calculation of reaction barriers,[36] was used to recalculate single point energies on optimized geometries. All calculations were done for *iso*-propanol solvent using COSMO implicit solvent model.[37,38]

The Gibbs free energy of reaction ΔG^0 and Gibbs free energy of activation $\Delta G^\ddagger$ at temperature of 60 °C were computed using the results of frequency analysis with B3LYP-D3(BJ) and corrected using DSD-BLYP-D3(BJ) electronic energy values. DSD-BLYP-D3(BJ) values are discussed in the paper, and B3LYP-D3(BJ) values are given in Supporting Information (SI) for comparison. The details of computational methods, the geometries of all calculated structures and corresponding free energy values are also provided in Supporting Information (SI), sections 1–3.

Microkinetic modelling was used to simulate reactions with catalysts **1** and **3** and to determine contribution of each reaction pathway (IS, OS, MPV) to the overall transfer hydrogenation rate.[39] Isothermal reaction conditions, the absence of concentration and temperature gradients and phase changes in the experimental liquid-phase batch catalytic reactor were assumed for catalyst **1**. The reaction mixture was considered an ideal solution.

A continuous stirred tank reactor (CSTR) model was used to describe reactions in the experimental batch reactor with homogeneous catalyst:

$$\frac{\mathrm{d}c_k}{\mathrm{d}t} = \frac{R_k N_{\mathrm{Ir}}}{V} \qquad (1)$$

$$\frac{\mathrm{d}y_s}{\mathrm{d}t} = R_s \qquad (2)$$

where c_k is the molar concentration of k^{th} species in the liquid, kmol/m^3, y_s is the molar fraction of catalyst species s (complex **1** or any Ir-containing species that can be produced from **1** according to the kinetic model), R_k is the formation/consumption rate for liquid species k, 1/s, R_s is the formation/consumption rate for catalyst species s, 1/s, V is the volume of liquid, m^3.

Species creation and consumption rates were calculated using microkinetic approach as explained in SI, section 4. Kinetic constants k_r were calculated using the Eyring equation with $\Delta G^{\ddagger}$ values taken from DFT results except for catalyst activation/deactivation reactions (see section “Kinetic modelling”).

Additional assumptions used in the modelling for catalyst **3**, with respect to modelling for catalyst **1**, were:

- No external mass transfer limitations, but mass-transfer limitations can be present in the near-surface layer;
- Some fraction of Ir species is inaccessible to the reaction;
- No Ir leaching;[9]
- The reaction kinetics for **1** and **3** are the same.

The calculation of the Damköhler number confirms the absence of external mass transfer limitations for the immobilized catalyst (SI, section 5). However, the significant linker length of the immobilized complex can influence the boundary layer structure near the polymer surface of the Wang resin and slow down the diffusion rate. The mass transfer coefficient in this near-surface layer is not known *a priori*, and possibly, it is not equal to the one in the liquid bulk, β_{bulk}. To account this, we have developed a mathematical model, which includes two zones: the liquid bulk and the near-surface layer. The thickness of this layer (2.5 nm) is estimated as a tethered catalyst length (SI, section 6). This value has no prominent effect on the results as changing the near-surface layer thickness from 2.5 nm to 250 nm changes the absolute conversion by less than 4% (SI, Table S5). For catalyst **3**, the model consists of Equations (2)–(4):

$$\frac{\mathrm{d}c_k}{\mathrm{d}t} = \frac{-\beta' S'(c_k - c_k^s)}{V_b} \qquad (3)$$

$$\frac{\mathrm{d}c_k^s}{\mathrm{d}t} = \frac{\beta' S'(c_k - c_k^s) + R_k N_{\mathrm{Ir}}}{V_s} \qquad (4)$$

where c_k^s is the molar concentration of k^{th} liquid species in the near-surface layer, kmol/m^3, V_s is the volume of liquid in the near-surface layer, m^3, V_b is the volume of liquid in the liquid bulk, m^3, $V = V_b + V_s$, β' is the mass transfer coefficient to the near-surface layer where the tethered catalyst is located, m/s, S' is the boundary layer surface area, m^2, N_{Ir} is the total loading of Ir in the reactor, kmol. In this case, y_s in [Eq. (2)] is referred to complex **3** or any Ir-containing species that can be produced from **3**.

Catalyst **1** is initially present as a dimer, whilst catalyst **2** is also dimeric but the coordination state of the supported catalyst **3** is not known.[10] Catalyst **3** is rigidly attached to the surface and it is hard to predict, which fraction of monomers can interact with each other and dimerize. To accommodate this into the model, an accessibility coefficient, γ, was introduced. It is defined as a fraction of Ir species involved in reactions for catalyst **3**. $(1 - \gamma)$ is the fraction of Ir inaccessible to the reaction due to dimerization, agglomeration, entanglement of tethers[9]. The initial state of **3** was taken as monomer.

The following model parameters from the experiment were used: temperature of 60 °C, liquid volume $V = 10$ ml, total iridium loading $N_{\mathrm{Ir}} = 0.02$ mmol for the homogeneous catalyst and $N_{\mathrm{Ir}}^{0} = 0.015$ mmol for the immobilized catalyst (0.3 mmol Ir/g, 50 mg). The amount of catalyst **3**, accessible to the reactions, was calculated as $N_{\mathrm{Ir}} = \gamma\, N_{\mathrm{Ir}}^{0}$. V_s in [Eq. (4)] was calculated using the near-surface layer thickness, particle diameter of 120 μm (SI, section 7) and assuming the catalyst layer porosity $\varepsilon = 0.5$.

Experimental Section

Details of the catalyst preparation and kinetic experiments are given in the SI, section 8.

Results and Discussion

Experimental results. The experimental results obtained for benzaldehyde transfer hydrogenation in a batch mode show that the five-carbon chain tether (C_5) does not affect the reaction rate significantly (Table 1, more data are provided in the SI, Table S6). So, one can assume the same reaction mechanism for $[Cp^*IrCl_2]_2$ dimer **1**, its tethered analogue **2** and the immobilized catalyst **3**. The estimated TOF for the immobilized catalyst **3** is 2.8 times lower than the one for $[Cp^*IrCl_2]_2$ (SI, section 9).

Table 1. Conversion of benzaldehyde by homogeneous and immobilized Ir complexes **1-3**.[a]

Entry	Catalyst	Conversion [%]		
		1 h	3 h	48 h
1	**1**	46.1	91.1	97.0
2	**2**	45.2	96.2	96.2
3	**3**	12.4	32.8	96.8[b]

[a] **1** or **2** (0.01 mmol), or 50 mg of **3** (0.3 mmol Ir/g, ICP), *t*BuOK (0.01 mmol), *i*PrOH (10 mL), 60 °C and 1 h stirring before adding benzaldehyde (1 mmol) = time 0 h. [b] Conversion at 12 h.

Catalyst activation and deactivation reactions. The homogeneous catalyst was used as the $[Cp^*IrCl_2]_2$ dimer **1**. The optimized geometry is in reasonable agreement with those obtained from experimental studies (SI, section 10). It is known that **1** breaks down into two Cp^*IrCl_2 monomers to become reactive.[10] DFT calculations predict free energy barrier of activation for this step $\Delta G^‡$ = 59.9 kJ/mol (45.6 kJ/mol for the reverse reaction). The dissociation constant K_p is 5.7×10^{-3} at 60 °C. Therefore, in the absence of reaction the dimer should be the predominant species in *iso*-propanol.

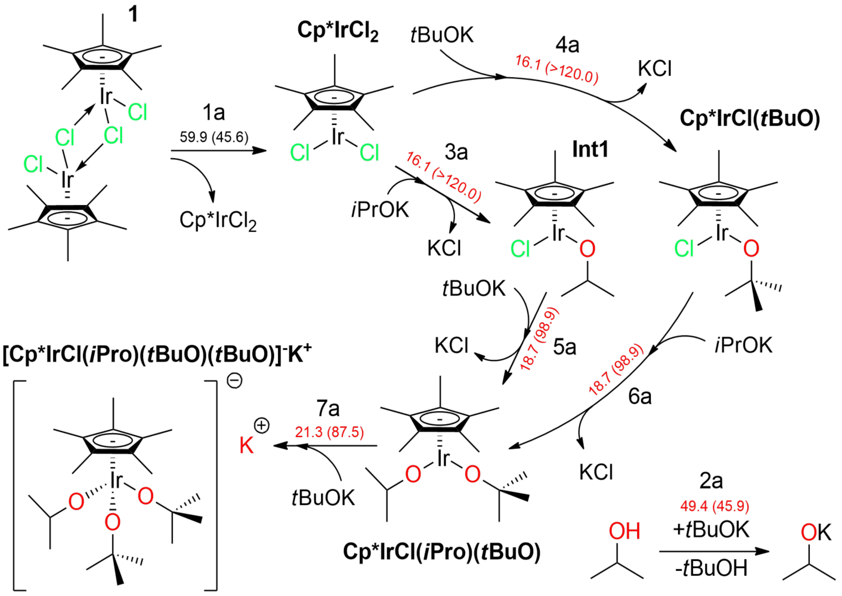

Scheme 3. Activation and deactivation reactions for transfer hydrogenation of benzaldehyde using [Cp*IrCl$_2$]$_2$ complex **1**. The values of free energy barriers (kJ/mol) are provided under reaction numbers. The barriers of reverse reactions are given in parentheses. Red numbers are fitted values.

Potassium *tert*-butoxide base is added to activate the catalyst. The interaction with base is complex and involves multiple steps. Moreover, potassium *tert*-butoxide can be present as tetramer. This leads to a number of possible reaction pathways and makes transition state search time-consuming and problematic. For this reason, we introduced overall reactions 2a–7a into the model, and fitted their kinetic parameters (see section "Kinetic modelling").

It is known that ~half the chloride ligands are lost during activation of the immobilized [Cp*IrCl$_2$]$_2$ complex, which is attributed to the replacement one chloride with alkoxide to give an Ir-alkoxide intermediate.[10] Both *iso*-propoxide and *tert*-butoxide anions can form alkoxide species with the catalyst (reactions 3a–4a, Scheme 3), however, only *i*PrO$^-$ can provide the hydride in the transfer step, required in all three reaction pathways. So, Cp*IrCl(*i*PrO) **Int1** is the common intermediate for these pathways. Catalyst deactivation can occur by over-reaction with alkoxide to replace both chloride ligands (reactions 5a–6a), and possible further reaction 7a to give the sterically crowded anionic Ir(III) complex with potassium counter-ion.[10]

Inner sphere mechanism. The IS mechanism starts with β-hydride elimination from alkoxide complex **Int1** to form **Int2** (Scheme 4, reaction 1i). A rather high energy barrier, 43.6 kJ/mol, must be overcome for the hydride transfer to iridium (Figure 1). According to Balcells *et al.*, a similar β-hydride elimination step with methanol and $CpIrCl_2$ catalyst has the highest barrier of 69.5 kJ/mol amongst all steps in the mechanism.[40] The reverse reaction has an energy barrier of 18.0 kJ/mol (2.5 kJ/mol to form methoxide[40]). The discrepancy with our values, are due to the difference in reaction temperature, H-donor, solvent and solvation model used in calculations.

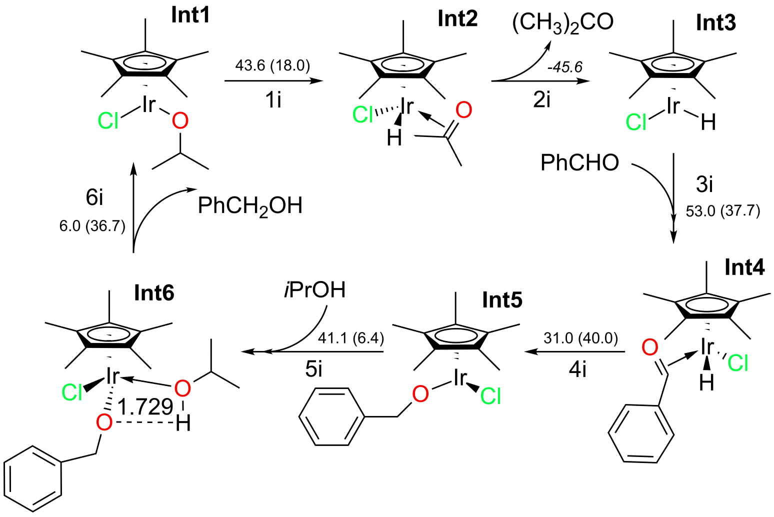

Scheme 4. Inner sphere mechanism of benzaldehyde hydrogenation using $[Cp^{*}IrCl_2]_2$ catalyst. Dotted lines depict hydrogen bonds. The values of free energy barriers (kJ/mol) are provided under reaction numbers. The barriers of reverse reactions are given in parentheses. Free energy differences are given in italics.

The Ir-O bond distance in **Int1** is 1.968 Å. Similar values of 2.015 Å[24] and 1.921 Å[40] were reported for the Ir-methoxide bond. The transition state of reaction 1i and the formed **Int2** species have syn-periplanar, almost rectangular, geometry, H-Ir-O-C, for the transferred hydrogen, iridium atom and carbonyl group (SI, section 11). The value of the Ir-O bond distance for **Int2** is 2.168 Å. This type of geometry was reported for the β-hydrogen elimination from square planar Ir(I) alkoxide complex.[41]

Removal of acetone in a barrierless step 2i is highly favourable (Figure 1). This leads to the hydride species Cp*IrCl(H) **Int3**. The strongest IR frequency for **Int3** (2092 cm^{-1}) lies in a range 2035-2130 cm^{-1} observed for a variety of hydride complexes Cp*IrPPh$_3$(*i*PrO)(H), Cp*IrPPh$_3$(EtO)(H), Cp*IrPPh$_3$(*n*PrO)(H), Cp*IrPPh$_3$(NHPh)(H).[42]

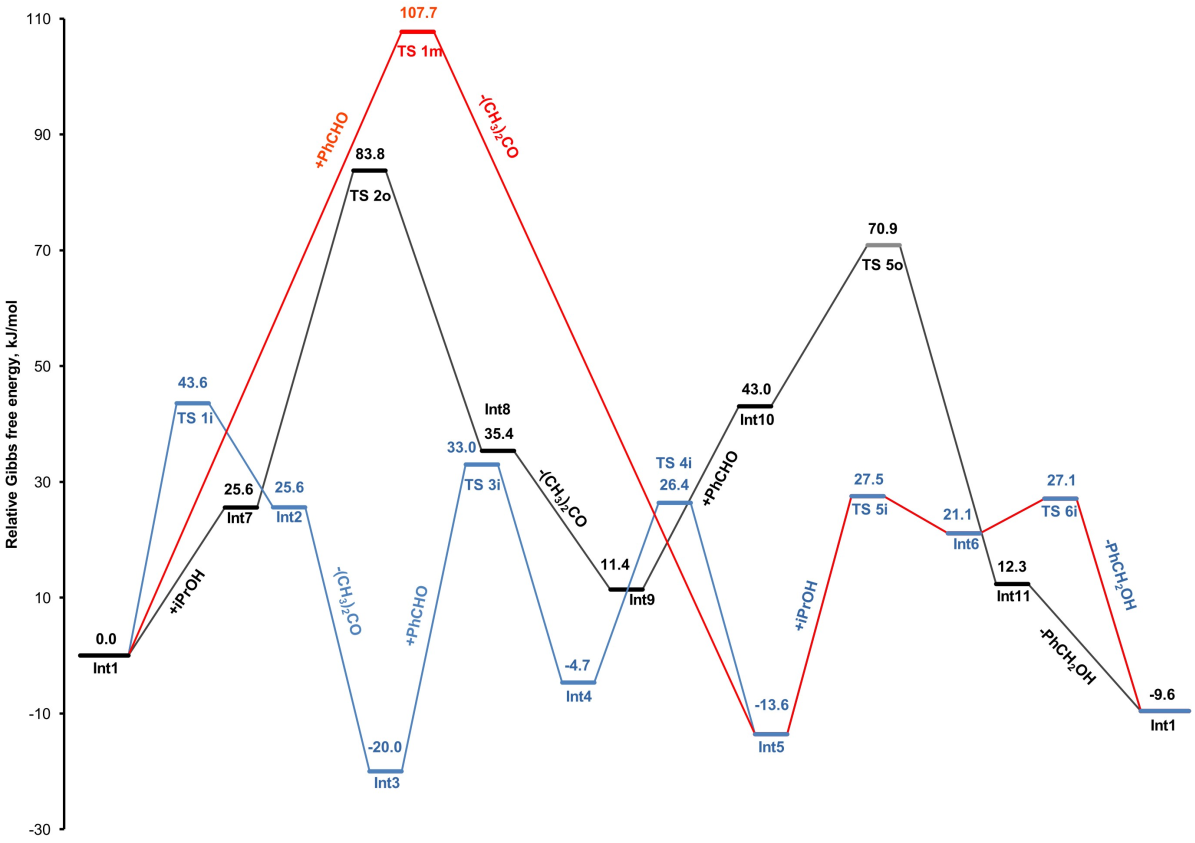

Figure 1. DFT-calculated free energy profile for the inner sphere (blue), outer sphere (black) and MPV (red) pathways of benzaldehyde hydrogenation.

Substrate coordination to **Int3** was studied from different initial positions. Two pathways, referred to as the main IS pathway (Scheme 4) and the alternative one (SI, section 12), were found. If benzaldehyde reaches **Int3** from one side of Ir-Cl-H(hydride) plane, namely, *Re* plane of Ir, the reaction results in **Int4**. If benzaldehyde reaches **Int3** from *Si* plane of Ir, the reaction results in **Int4'**. The main IS pathway goes through intermediates **Int4**, **Int5** and **Int6**. The alternative IS pathways goes through intermediates **Int4'**, **Int5'** and **Int6'**, which are enantiomers of the corresponding intermediates in the main IS pathway. The two pathways are connected by a low-barrier ligand rotation reaction 7i (~8 kJ/mol) and are close in energy (SI, section 12), so only the main pathway, which is a bit lower in energy, is discussed below.

Benzaldehyde coordination to Ir leads to syn-periplanar geometry H-Ir-O-C in **Int4**, which resembles the geometry of **Int2** (SI, section 11). The value of the Ir-C distance (2.211 Å) is close to the value of Ir-O distance (2.133 Å) in **Int4**, which provides evidence for the π-bound ligand (Scheme 4). This type of bonding with the metal also occurs for other C=O containing systems.[40] C=O distance for the coordinated benzaldehyde (1.296 Å) is much higher than for a single benzaldehyde molecule in a solvent (1.216 Å). A high barrier of reaction 3i (53.0 kJ/mol) may be caused by the high stability of the hydride and by steric effects.

The hydride transfer to benzaldehyde occurs with a barrier *via* a four-membered transition state of reaction 4i. The reverse β-hydride elimination requires to overcome a free energy barrier of 40.0 kJ/mol. This value is close to that for the *i*PrO$^-$ligand (1i). Both hydride transfer steps 1i and 4i, of the IS mechanism, have lower energy barriers than the coordination of benzaldehyde (3i, 53.0 kJ/mol, Figure 1).

For the proton transfer, NEB predicts two subsequent steps. The first one is *iso*-propanol coordination (5i, 41.1 kJ/mol). **Int6** is stabilized by the formation of hydrogen bond (Scheme 4).

The second step is proton transfer and benzyl alcohol removal. It requires only 6.0 kJ/mol (Figure 1).

It is important to consider that the highest energy barrier does not always determine the reaction kinetics, rather the effective reaction barrier is important. To find this, we followed the procedure described by Murdoch.[43] The energy profile is divided into parts, moving from left to right on the profile. The intermediate, which is lower in energy than all previous intermediates, is the starting point for the new part. In Figure 1, we have two parts to the profile, starting from **Int1** and **Int3**. For each part, the free energy difference between the highest and lowest point in the profile is calculated and the maximum difference is the effective barrier.[43] For the IS mechanism, the effective reaction barrier is the difference in energy between TS 3i and **Int3** (53.0 kJ/mol).

Outer sphere mechanism. An oxygen atom is usually considered as the active site for proton transfer in OS mechanism when bound indirectly to the metal. For example, in Shvö's catalyst the oxygen atom is embedded in the modified Cp ligand.[44,45] **Int1** provides the metal-bound oxygen atom, which may also be the active site for proton transfer. We studied only the concerted TS because this is facilitated when the oxygen atom is close to the metal site.[21]

The catalytic cycle of the outer sphere mechanism begins with *iso*-propanol H-bonding to alkoxide oxygen (**Int7**) in reaction 1o (Figure 1 and Scheme 5). Hydrogen transfer to the catalyst occurs through a high-energy six-membered concerted transition state (58.2 kJ/mol, reaction 2o). This transfer is asynchronous (SI, section 13). The acetone formed readily detaches in reaction 3o.

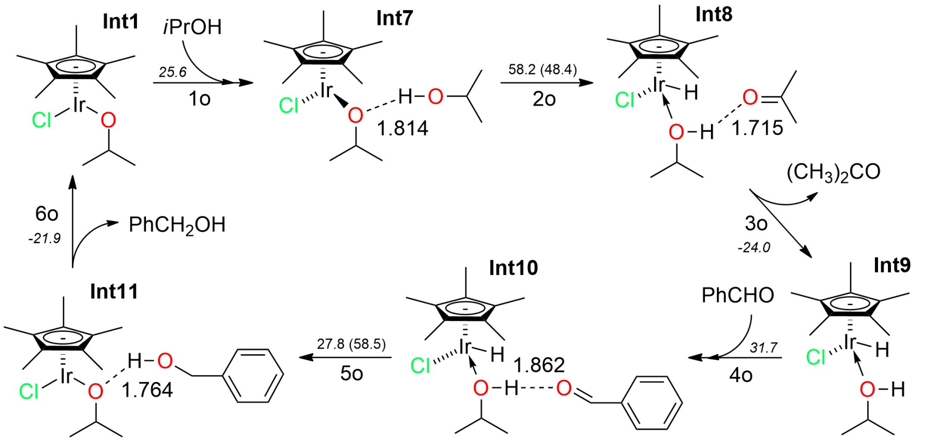

Scheme 5. Outer sphere mechanism of benzaldehyde hydrogenation using $[Cp^*IrCl_2]_2$ catalyst. Notation is the same as in Scheme 4.

Benzaldehyde interacts with **Int9** forming a hydrogen bond with hydroxyl group of *iso*-propanol (reaction 4o). Hydride transfer step 5o has a 27.8 kJ/mol free energy barrier, the reverse reaction being much more difficult. The hydrogen bond between benzyl alcohol and bound *iso*-propoxide then breaks with a free energy difference -21.9 kJ/mol in 6o (Scheme 5) to regain **Int1**.

The effective reaction barrier for the OS pathway is 83.8 kJ/mol. The first part of OS catalytic cycle, *iso*-propanol dehydrogenation, is more difficult than benzaldehyde hydrogenation. The six-membered TS, step 2o, involving hydrogen transfer from *iso*-propanol to *iso*-propoxide anion has the highest relative energy in this pathway.

MPV mechanism. In the MPV mechanism, the lowest energy pathway was found to include benzaldehyde coordination with the simultaneous direct hydrogen transfer and acetone removal (Scheme 6). This process is energy demanding (107.7 kJ/mol). However, the reverse reaction is more difficult to proceed (121.3 kJ/mol). The rest of the pathway coincides with the IS pathway (reactions 5i and 6i). The effective reaction barrier for MPV pathway is 107.7 kJ/mol.

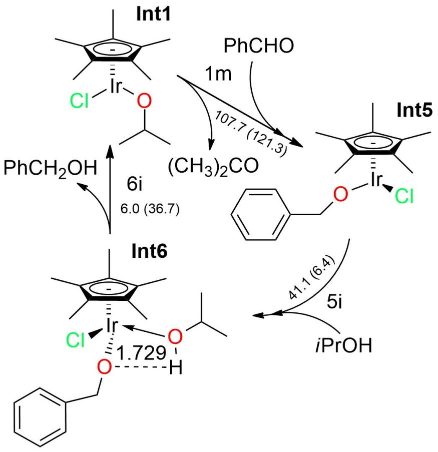

Scheme 6. MPV mechanism of benzaldehyde hydrogenation using [Cp*IrCl$_2$]$_2$ catalyst. Notation is the same as in Scheme 4.

Comparison of the three mechanisms. Comparing the values of the effective free energy reaction barriers, it can be concluded that the inner sphere mechanism is the most favourable (53.0 kJ/mol). Its effective barrier is a barrier of coordination of benzaldehyde, the highest barrier in the IS mechanism. Hydride transfer to Ir has the second highest barrier (1i, 43.0 kJ/mol). In contrast to the hydride transfer, the proton transfer has a low energy barrier (6.0 kJ/mol), which is common for hydrogen transfer reactions.[46] The MPV mechanism has the highest effective energy barrier and is the least favourable.

Kinetic modelling. The Gibbs free energy reaction barrier values in the Eyring equation were taken from the DFT results for catalyst **1** (SI, section 3). We augmented the reaction set studied by DFT (1i–7i, 3i’–6i’, 1o–6o, 1m, 1m’, 1a) with catalyst activation and deactivation reactions (2a–7a, Scheme 3). The same kinetic model was used to simulate reactions with catalyst **3**, except reaction 1a.

Free energy barrier values for reactions 2a–7a were fitted in mech_optimiz software[47,48] using the experimental data for catalysts **1** and **3** (SI, Table S6). Reactions 3a and 4a, 5a and 6a, are similar. One of the reactions in each pair is an exchange of Cl^- ligand with $iPrO^-$, and the other one is an exchange of Cl^- ligand with $tBuO^-$. One may expect that the values of reaction barriers are very close for the reactions in each pair, either in the forward direction (subscript "f") or in the backward one (subscript "b"). Thus, the following constraints were imposed on the free energy barriers: $\Delta G^{\ddagger}_{3a,f} = \Delta G^{\ddagger}_{4a,f}$, $\Delta G^{\ddagger}_{3a,b} = \Delta G^{\ddagger}_{4a,b}$, $\Delta G^{\ddagger}_{5a,f} = \Delta G^{\ddagger}_{6a,f}$, $\Delta G^{\ddagger}_{5a,b} = \Delta G^{\ddagger}_{6a,b}$. The objective function for fitting was a residual sum of squares between the experimental and simulated benzaldehyde conversion values. This objective function was minimized using an advanced genetic algorithm with automatic reinitialization when converging to a local minimum (SI, section 14).[47,48]

In addition, the parameters β' and γ were fitted for catalyst **3**; β' in the range between the diffusion coefficient in the bulk liquid (β_{bulk}~5.4×10^{-4}, SI, section 5) and 10^{-10} and γ between 0.1 and 1. To calculate benzaldehyde conversion, Equations (1) and (2) for catalyst **1** or Equations (2)-(4) for catalyst **3** were solved sequentially for the activation period and the reaction period. Conversion data were calculated only for the reaction period due to the absence of substrate during the catalyst activation.

The best fit was obtained with $\gamma = 0.226$. It means that 22.6% of the Ir complexes are accessible for reaction. The simulated and experimental conversion values agree well for both the homogeneous and the immobilized catalysts (Figure 2).

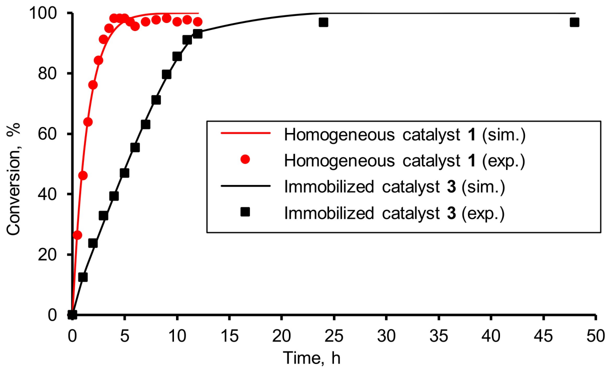

Figure 2. Comparison of simulation results and experimental data for benzaldehyde conversion over homogeneous and immobilized Ir complexes. Reaction simulation conditions: the same as in Table 1.

The order of error in DFT values can be quantified using the value of Gibbs free energy change of overall hydrogen transfer reaction of benzaldehyde with isopropanol. The absolute value of DFT error in Gibbs free energy change for this reaction is equal to ~ 10.2 kJ/mol (SI, section 15). This error is comparable to the mean absolute error of DSD-BLYP-D3(BJ) functional for reactions of large systems using GMTKN55 database (2.22 kcal/mol[49]). We estimated the uncertainty in γ value changing Gibbs free energy values for the transition states of rate-controlling steps 1i, 3i and 3i' by 10 kJ/mol. The results show that γ lies in a rather narrow [0.226; 0.2425] range (SI, section 16).

The simulated equilibrium conversion 99.98% is predicted by DFT-based equilibrium calculations (99.06 % using tabulated thermodynamic data, SI, section 15). However, this was not achieved experimentally both for catalyst **1** (98.0 %) and catalyst **3** (96.8 %), perhaps due to side-reactions such as the Cannizzaro reaction. For β', interval estimate was obtained, $10^{-7} \leq \beta' \leq \beta_{\text{bulk}}$. In this range, the reaction rate is insensitive to changes in the near-surface layer mass transfer coefficient (SI, section 17). These results confirm the absence of mass transfer limitations, and one may take $\beta' = \beta_{\text{bulk}}$.

The energy barrier to exchange one Cl ligand for the *iso*-propoxide anion is estimated as 16.1 kJ/mol, but the reverse reaction has a large barrier over 120 kJ/mol (SI, Table S9). The second chloride ligand can be exchanged with a similar energy barrier of 18.7 kJ/mol (reverse reaction 98.9 kJ/mol), making it more difficult to exchange than the first. Nevertheless, the low energy barriers for Cl replacement with alkoxide, and high reverse barriers, imply that the catalyst could be mainly in a deactivated state, particularly with *tert*-butoxide.

Calculation of the reaction rates with catalyst **1** gives a dimensionless instantaneous reaction rate (site-time yield) equal to ~0.0036 s^{-1} after 1 h of reaction for the inner sphere mechanism. This value is a total contribution of the main and the alternative IS pathways. The values of reaction rates for the OS and the MPV pathways are below 10^{-8} and 10^{-14} s^{-1}, respectively. The latter holds for the catalyst **3**. Thus, the results suggest that the inner sphere mechanism is the only one operating at 60 °C.

The reaction path analysis for catalyst **3** reveals that both the main IS pathway and the alternative IS pathway contribute substantially to the conversion (SI, figure S8). This results from the close values of effective barriers of the two (64.3 kJ/mol and 67.8 kJ/mol, respectively, SI, section 12). Taking into account DFT geometry tolerances and energy errors, one may consider benzaldehyde binding to **Int3** from the different sides of Ir-Cl-H plane equally probable.

Degrees of rate control are commonly used as indicators of rate-limiting steps.[50,51] The greater the value of degree of rate control for some reaction, the greater the impact has the transition state energy of this reaction on the overall reaction rate. We have calculated the degree of conversion control[51] $X_{\mathrm{cc},u}$ for the transfer hydrogenation of benzaldehyde in a batch reactor with complex **3** at reaction time 1 h (Table 2):

$$X_{\mathrm{CC},u}=\frac{k_u}{x}\left(\frac{\partial x}{\partial k_u}\right)_{k_{j\neq u},K_u} \qquad (5)$$

where x is benzaldehyde conversion, %, k_u is a kinetic constant of reaction u, which is changed whilst keeping the kinetic constants of the other reactions $k_{j\neq u}$ unchanged and preserving the value of the equilibrium constant K_u.

Table 2. Dimensionless sensitivity coefficients and degrees of conversion control for the inner sphere reaction pathway, activation and deactivation reactions after 1 h of reaction using catalyst **3**[a]

Reaction	$S_{u,f}$	$S_{u,b}$	$X_{CC,u}$
2a	0.67	-0.37	0.30
4a	-0.10	1.7×10^{-3}	-0.10
5a	-0.57	0.86	0.29
1i	0.56	-2.1×10^{-3}	0.56
3i	0.30	-6.4×10^{-2}	0.23
3i’	0.12	-4.1×10^{-2}	0.08

[a] Reaction conditions for simulation: the same as in Table 1. Data are provided only for reactions with absolute values of sensitivity coefficients higher than 0.1.

One way to calculate the degree of control is changing the forward and backward kinetic constants of reaction u separately, then summing up the dimensionless sensitivity coefficients [Eq. (6)]:[52]

$$S_{u,f}=\frac{k_{u,f}}{x}\left(\frac{\partial x}{\partial k_{u,f}}\right)_{k_{j\neq u},k_{u,b}}$$

$$S_{u,b}=\frac{k_{u,b}}{x}\left(\frac{\partial x}{\partial k_{u,b}}\right)_{k_{j\neq u},k_{u,f}}$$

$$X_{CC,u} = S_{u,f} + S_{u,b} \qquad (6)$$

where ∂k_u is a change in kinetic constant, ∂x is the corresponding change in benzaldehyde conversion. We used $\partial k_u = -0.01k_u$ that corresponds to the increase of transition state Gibbs free energy of reaction u, G_u^{TS}, by 27.8 J/mol at the reaction conditions studied.

TS 1i, TS 3i and TS 3i’ noticeably influence the overall rate ($X_{cc,u} > 0.1$, Table 2). These transition states correspond to the rate-limiting steps in the IS mechanism. Our results show that both the highest transition state (TS 1i) and the most stable intermediate (**Int 3**) that determine the energy span, also determine the reaction rate in the IS mechanism. Transition state TS 1i has the strongest effect on the overall rate ($X_{cc} = 0.56$). It is hydride transfer from isopropanol to the catalyst, which mainly limits the reaction rate.

Int3 Cp*IrCl(H) is the most abundant reaction intermediate amongst intermediates **Int1**–**Int11** both for catalyst **1** and catalyst **3** (Table 3). However, high sensitivity coefficients and degree of rate control of reaction **5a** make deactivated species much more abundant. Clearly, catalyst deactivation is a very important process because it controls the number of active sites available for the reaction.

Table 3. Catalyst species mole fraction in transfer hydrogenation of benzaldehyde.[a]

Catalyst	State (kind of catalyst species)	Species fraction	
		1 h	12 h
1	$(Cp^*IrCl_2)_2$	0.464	0.464
1	Cp*IrCl(*t*BuO)	0.498	0.498
1	Cp*Ir(*i*PrO)(*t*BuO)	1.0×10^{-3}	1.0×10^{-3}
1	Cp^*IrCl_2	0.036	0.036
1	Cp*IrCl(H)	3.5×10^{-5}	4.3×10^{-5}

3	Cp*Ir(*i*PrO)(*t*BuO)(*t*BuO)(K)	0.859	0.859
3	Cp*Ir(*i*PrO)(*t*BuO)	0.141	0.141
3	Cp*IrCl(H)	3.3×10^{-5}	1.6×10^{-4}

[a] Simulation conditions: the same as in Table 1.

The resting state for both the catalyst **1** and the catalyst **3** is deactivated species. The homogeneous catalyst **1** exists mainly as an inactive dimer (Table 3). The fraction of monomer is below 0.04. Interestingly, the simulation predicts different deactivated species as predominant for catalysts 1 and 3. About a half of the catalyst 1 exists as deactivated alkoxide species Cp*IrCl(*t*BuO). The immobilized catalyst **3** exists mainly as the strongly deactivated species Cp*Ir(*i*PrO)(*t*BuO)(*t*BuO)(K) with potassium counter-ion, observed experimentally.[10] The fraction of **Int3** species increases in time for **1** as well as for **3**, indicating that these catalysts are more active after the 12 h batch reaction than before. An increase in reaction rate for the second batch was previously observed for catalyst **3**.[8] This may lead to understanding how to improve activity of the immobilized catalyst.

Reactions 3a–7a are very important, because they control catalyst activation and deactivation. Changing the rate of catalyst deactivation will change the concentration of deactivated species, and also the number of Cp*IrCl(H) species involved into the catalytic turnover. Since potassium *tert*-butoxide is involved in the activation and deactivation processes, its concentration is expected to affect the rate strongly. The results of simulation for catalyst **3** show that there is an optimal amount of base (Table 4). In our system, it is equal to 0.8-0.9 mM depending on reaction conditions, and the respective catalyst/base ratio is ~ 1.8.

Table 4. The effect of base and substrate concentration on benzaldehyde conversion for catalyst **3**. Simulation conditions: *i*PrOH (10 mL), 60 °C, 1 h stirring before the reaction, 12 h.

Catalyst, mM	Substrate, M	Base, mM	Conversion, %		
			1 h	5 h	7 h
1.5	0.1	0.4	18.3	95.6	99.85
		0.8	23.3	98.7	99.97
		0.85	24.9	99.2[a]	99.97
		0.9	26.4	98.9	99.97
		0.95	23.5	91.3	99.10
		1.0	12.3	48.2	64.5
3.0	0.1	1.0	39.9	99.96	99.98
		1.8	71.5	99.98	99.98
		2.0	23.6	73.7	91.0
1.5	0.2	0.8	18.7	95.8	99.90
		0.9	20.9	95.3	99.80
		1.0	7.6	26.7	36.1

[a] Values marked with green indicate the best conversion at specific conditions and time

The optimal catalyst/base ratio is almost independent of the substrate concentration and is related to the change in hydride **Int3** concentration (Figure 3). The maximum substrate conversion is in line with the maximum hydride concentration, which is a function of base concentration. This was also shown for acetophenone hydrogenation with *iso*-propanol on [(mesitylene)((*R*,*R*)-TsDPEN)-RuCl] catalyst with KOH base.[53] An excess of base is detrimental to the activity because of strong catalyst deactivation and a decrease in hydride concentration (Figure 3, 1.0 mM base). Too small amount of potassium *tert*-butoxide makes the rate too low because of slow hydride generation.

Usage of the optimal amount of base provides a compromise between catalyst activation and deactivation processes and the most rapid generation of hydride species under reactive conditions.

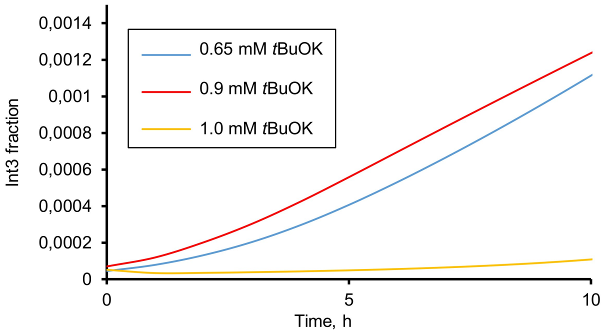

Figure 3. The effect of base concentration on fraction of catalyst **3** in a hydride state **Int3**. Simulation conditions: the same as in Table 1, base concentration varies.

The amount of base is clearly a critical parameter to determine experimentally. From our previous work, the use of hindered amine rather than alkoxide bases has potential in *iso*-propanol mediated transfer hydrogenation.[9]

Conclusion

The mechanism of benzaldehyde transfer hydrogenation using *iso*-propanol with the homogeneous $[Cp^{*}IrCl_2]_2$ catalyst **1** has been investigated. It has been shown that incorporation of C_5 tether into **1** does not significantly change the reaction rate, and it is likely that **1** and **2** undergo under the same mechanism. Also, the same mechanism can be assumed for **3**. Our DFT calculations for catalyst **1** predict that the inner sphere mechanism is totally favoured over the outer sphere or MPV mechanisms. The estimated effective barrier of the IS pathway is 53.0 kJ/mol.

The proposed variant of the outer sphere mechanism with alkoxide-oxygen mediated proton transfer, has a large effective barrier 83.8 kJ/mol. The main reason for this is the six-membered concerted transition state of hydrogen transfer from *iso*-propanol to Ir is high in energy and disfavoured. The MPV mechanism has a largest effective barrier of 107.7 kJ/mol, which is consistent with the general viewpoint that hydridic mechanisms, and not direct transfer, are usually favourable for Ru and Ir catalysts in aqueous and organic media.[17,54]

Amongst the IS mechanism reactions, benzaldehyde coordination to iridium (3i) and β-hydride elimination from alkoxide complex **Int1** (1i) have the strongest effect on the transfer hydrogenation rate for catalyst **3**. These reactions are related to the highest transition state and the lowest intermediate in terms of Gibbs free energy. Outside the IS pathway, reactions 2a, 4a and 5a have high values of degrees of conversion control as they control the activation and deactivation rates.

The results of DFT-assisted microkinetic modelling show that hydride species Cp*IrCl(H) concentration is related to the activity of the immobilized catalyst and is a function of base concentration. 0.8-0.9 mM of potassium *tert*-butoxide is optimal when using 1.5 mM of catalyst **3**. Nevertheless, our study suggests that most of the catalysts **1** and **3** exists as non-reactive species: **1** mainly exists as a dimer and Cp*IrCl(*t*BuO) species and **3** mainly exists as a deactivated alkoxide species without chlorine ligands, Cp*Ir(*i*PrO)(*t*BuO)(*t*BuO)(K).

The best parameter fitting predicts that only about a quarter of Ir complexes **3** are involved into reaction, and this is the main reason for the observed difference in activity of **1** and **3**. The most probable reasons for the low involvement are entanglement of tethers, dimerization and deactivation of immobilized catalyst. This is supported by the fact that the mean distance between species **3** on the polymer surface is estimated to be much less than the length of **3** (SI, section 18). The simulation supports the fact that mass-transfer limitations are not present for catalyst **3** in a batch CSTR, and they are not responsible for lower TOF values for **3** with respect to **1**.

The results indicate the importance of potassium *tert*-butoxide base concentration for transfer hydrogenation of aromatic substrates on homogeneous and immobilized catalysts. The use of another base, such as Et_3N, which has a lower catalyst deactivation effect, should also be considered.[9]

This work is the one of the first examples of the use of microkinetic modelling in liquid phase catalysis, both homogenous and heterogeneous. We hope that both microkinetic approach and the reactor models developed will be used to study other liquid phase catalytic reactions.

Supporting Information.

Computational details (section 1), calculated geometries (section 2), free energy of activation for all reaction steps studied (section 3), equations for calculation of reaction rates (section 4), assessment of possibility of external mass transfer limitations existence for the immobilized catalyst in CSTR (section 5), calculation of effect of near-surface layer thickness on benzaldehyde conversion for the immobilized catalyst (section 6), SEM data for the immobilized catalyst (section 7), catalyst synthesis and experimental kinetics study details (section 8), calculation of TOF (section 9), comparison of selected experimental and calculated bond distances and angles for $(Cp^*IrCl_2)_2$ complex (section 10), 3D geometry of selected species (section 11), the alternative IS and MPV pathways (section 12), the nature of hydrogen transfer in OS mechanism (section 13), kinetic parameter fitting details (section 14), equilibrium calculation for the reaction between isopropanol and benzaldehyde (section 15), study of uncertainty in fitted parameters due to DFT error (section 16), the dependence of benzaldehyde conversion on mass transfer coefficient in the near-surface layer (section 17), the estimation of distance between species of immobilized catalyst on the polymer support (section 18) are available free of charge as PDF file via Internet at https://pubs.acs.org.

Corresponding Author

* mitrichev.i.i@muctr.ru

Present Addresses

† Chemical Process R&D, CMC & Production HQs, Ono Pharmaceutical Co., Ltd. 3–1–1 Sakurai, Shimamoto–Cho, 618–8585 Osaka, Mishima–Gun (Japan)

Notes

The authors declare no conflict of interest.

Acknowledgements

Financial support was provided by the British Council and Newton Institutional Links UK-Russia project 277335368 (IM, MC, MV, AP, EK). The work was partly performed in the framework of the development program «Priority-2030» of the Mendeleev University of Chemical Technology of Russia (IM, EK). We would like to thank Ono Pharmaceutical, Japan for the secondment of YK to the iPRD. We thank prof. Vladimir Tsirelson (Mendeleev University of Chemical Technology of Russia) and prof. Maria Khrenova (Moscow State University) for their advices.

References

(1) Wang, D.; Astruc, D. The Golden Age of Transfer Hydrogenation. *Chem. Rev.* **2015**, *115* (13), 6621–6686. https://doi.org/10.1021/acs.chemrev.5b00203.

(2) Andrushko, N.; Andrushko, V. Asymmetric Hydrogenation of C=O and C=N Bonds in Stereoselective Synthesis. In *Stereoselective Synthesis of Drugs and Natural Products*; Andrushko, V., Andrushko, N., Eds.; John Wiley & Sons, Inc.: Hoboken, NJ, USA, 2013; pp 909–960. https://doi.org/10.1002/9781118596784.ssd030.

(3) Klingler, F. D. Asymmetric Hydrogenation of Prochiral Amino Ketones to Amino Alcohols for Pharmaceutical Use. *Acc. Chem. Res.* **2007**, *40* (12), 1367–1376. https://doi.org/10.1021/ar700100e.

(4) Foubelo, F.; Nájera, C.; Yus, M. Catalytic Asymmetric Transfer Hydrogenation of Ketones: Recent Advances. *Tetrahedron Asymmetry* **2015**, *26* (15–16), 769–790. https://doi.org/10.1016/j.tetasy.2015.06.016.

(5) Blacker, A. J.; Thompson, P. Scale-Up Studies in Asymmetric Transfer Hydrogenation. In *Asymmetric Catalysis on Industrial Scale*; Blaser, H.-U., Federsel, H.-J., Eds.; Wiley-VCH Verlag GmbH & Co. KGaA: Weinheim, Germany, 2010; pp 265–290. https://doi.org/10.1002/9783527630639.ch16.

(6) Ikariya, T.; Blacker, A. J. Asymmetric Transfer Hydrogenation of Ketones with Bifunctional Transition Metal-Based Molecular Catalysts. *Acc. Chem. Res.* **2007**, *40* (12), 1300–1308. https://doi.org/10.1021/ar700134q.

(7) Fujita, K. I.; Yamaguchi, R. Cp*Ir Complex-Catalyzed Hydrogen Transfer Reactions Directed toward Environmentally Benign Organic Synthesis. *Synlett* **2005**, No. 4, 560–571. https://doi.org/10.1055/s-2005-862381.

(8) Lucas, S. J.; Crossley, B. D.; Pettman, A. J.; Vassileiou, A. D.; Screen, T. E. O.; Blacker, A. J.; McGowan, P. C. A Robust Method to Heterogenise and Recycle Group 9 Catalysts. *Chem. Commun.* **2013**, *49* (49), 5562–5564. https://doi.org/10.1039/c3cc42550a.

(9) Kawakami, Y.; Borissova, A.; Chapman, M. R.; Goltz, G.; Koltsova, E.; Mitrichev, I.; Blacker, A. J. Continuous Flow Asymmetric Transfer Hydrogenation with Long Catalyst

Lifetime and Low Metal Leaching. *European J. Org. Chem.* **2019**, *2019* (45), 7499–7505. https://doi.org/10.1002/ejoc.201901547.

(10) Sherborne, G. J.; Chapman, M. R.; Blacker, A. J.; Bourne, R. A.; Chamberlain, T. W.; Crossley, B. D.; Lucas, S. J.; McGowan, P. C.; Newton, M. A.; Screen, T. E. O.; et al. Activation and Deactivation of a Robust Immobilized Cp*Ir-Transfer Hydrogenation Catalyst: A Multielement *in Situ* X-Ray Absorption Spectroscopy Study. *J. Am. Chem. Soc.* **2015**, *137* (12), 4151–4157. https://doi.org/10.1021/ja512868a.

(11) Grajciar, L.; Heard, C. J.; Bondarenko, A. A.; Polynski, M. V.; Meeprasert, J.; Pidko, E. A.; Nachtigall, P. Towards Operando Computational Modeling in Heterogeneous Catalysis. *Chem. Soc. Rev.* **2018**, *47* (22), 8307–8348. https://doi.org/10.1039/c8cs00398j.

(12) Besora, M.; Maseras, F. Microkinetic Modeling in Homogeneous Catalysis. *Wiley Interdiscip. Rev. Comput. Mol. Sci.* **2018**, *8* (6), e1372. https://doi.org/10.1002/wcms.1372.

(13) Gu, G. H.; Wittreich, G. R.; Vlachos, D. G. Microkinetic Modeling of Aqueous Phase Biomass Conversion: Application to Ethylene Glycol Reforming. *Chem. Eng. Sci.* **2019**, *197*, 415–418. https://doi.org/10.1016/j.ces.2018.12.036.

(14) Faheem, M.; Saleheen, M.; Lu, J.; Heyden, A. Ethylene Glycol Reforming on Pt(111): First-Principles Microkinetic Modeling in Vapor and Aqueous Phases. *Catal. Sci. Technol.* **2016**, *6* (23), 8242–8256. https://doi.org/10.1039/c6cy02111e.

(15) Maestri, M. Microkinetic Analysis of Complex Chemical Processes at Surfaces. In *New Strategies in Chemical Synthesis and Catalysis*; Pignataro, B., Ed.; Wiley-VCH, 2012; pp 219–245. https://doi.org/10.1002/9783527645824.ch10.

(16) Samec, J. S. M.; Bäckvall, J. E.; Andersson, P. G.; Brandt, P. Mechanistic Aspects of Transition Metal-Catalyzed Hydrogen Transfer Reactions. *Chem. Soc. Rev.* **2006**, *35* (3), 237–248. https://doi.org/10.1039/b515269k.

(17) Iglesias, M.; Oro, L. A. A Leap Forward in Iridium-NHC Catalysis: New Horizons and Mechanistic Insights. *Chem. Soc. Rev.* **2018**, *47* (8), 2772–2808. https://doi.org/10.1039/c7cs00743d.

(18) Pàmies, O.; Bäckvall, J. E. Studies on the Mechanism of Metal-Catalyzed Hydrogen Transfer from Alcohols to Ketones. *Chem. - A Eur. J.* **2001**, *7* (23), 5052–5058. https://doi.org/10.1002/1521-3765(20011203)7:23<5052::AID-CHEM5052>3.0.CO;2-Z.

(19) Popoola, S. A.; Jaseer, E. A.; Al-Saadi, A. A.; Polo, V.; Casado, M. A.; Oro, L. A. Iridium Complexes as Catalysts in the Hydrogen Transfer of Isopropanol to Acetophenone: Ligand Effects and DFT Studies. *Inorganica Chim. Acta* **2015**, *436*, 146–151. https://doi.org/10.1016/j.ica.2015.07.031.

(20) Albrecht, M.; Miecznikowski, J. R.; Samuel, A.; Faller, J. W.; Crabtree, R. H. Chelated Iridium(III) Bis-Carbene Complexes as Air-Stable Catalysts for Transfer Hydrogenation. *Organometallics* **2002**, *21* (17), 3596–3604. https://doi.org/10.1021/om020338x.

(21) Eisenstein, O.; Crabtree, R. H. Outer Sphere Hydrogenation Catalysis. *New J. Chem.* **2013**, *37* (1), 21–27. https://doi.org/10.1039/c2nj40659d.

(22) Hintermair, U.; Campos, J.; Brewster, T. P.; Pratt, L. M.; Schley, N. D.; Crabtree, R. H. Hydrogen-Transfer Catalysis with Cp*IrIII Complexes: The Influence of the Ancillary Ligands. *ACS Catal.* **2014**, *4* (1), 99–108. https://doi.org/10.1021/cs400834q.

(23) Jiménez, M. V.; Fernández-Tornos, J.; Pérez-Torrente, J. J.; Modrego, F. J.; García-Orduña, P.; Oro, L. A. Mechanistic Insights into Transfer Hydrogenation Catalysis by [Ir(Cod)(NHC)2]+ Complexes with Functionalized N-Heterocyclic Carbene Ligands. *Organometallics* **2015**, *34* (5), 926–940. https://doi.org/10.1021/om5013083.

(24) Handgraaf, J. W.; Reek, J. N. H.; Meijer, E. J. Iridium(I) versus Ruthenium(II). A Computational Study of the Transition Metal Catalyzed Transfer Hydrogenation of Ketones. *Organometallics* **2003**, *22* (15), 3150–3157. https://doi.org/10.1021/om030104t.

(25) Neese, F. The ORCA Program System. *Wiley Interdiscip. Rev. Comput. Mol. Sci.* **2012**, *2* (1), 73–78. https://doi.org/10.1002/wcms.81.

(26) Schäfer, A.; Horn, H.; Ahlrichs, R. Fully Optimized Contracted Gaussian Basis Sets for Atoms Li to Kr. *J. Chem. Phys.* **1992**, *97* (4), 2571–2577. https://doi.org/10.1063/1.463096.

(27) Weigend, F.; Ahlrichs, R. Balanced Basis Sets of Split Valence, Triple Zeta Valence and Quadruple Zeta Valence Quality for H to Rn: Design and Assessment of Accuracy. *Phys. Chem. Chem. Phys.* **2005**, *7* (18), 3297–3305. https://doi.org/10.1039/b508541a.

(28) Andrae, D.; Häußermann, U.; Dolg, M.; Stoll, H.; Preuß, H. Energy-Adjusted Ab Initio Pseudopotentials for the Second and Third Row Transition Elements. *Theor. Chim. Acta* **1990**, *77* (2), 123–141. https://doi.org/10.1007/BF01114537.

(29) Weigend, F. Accurate Coulomb-Fitting Basis Sets for H to Rn. *Phys. Chem. Chem. Phys.* **2006**, *8* (9), 1057–1065. https://doi.org/10.1039/b515623h.

(30) Becke, A. D. Density-Functional Thermochemistry. III. The Role of Exact Exchange. *J. Chem. Phys.* **1993**, *98* (7), 5648–5652. https://doi.org/10.1063/1.464913.

(31) Grimme, S.; Ehrlich, S.; Goerigk, L. Effect of the Damping Function in Dispersion Corrected Density Functional Theory. *J. Comput. Chem.* **2011**, *32* (7), 1456–1465. https://doi.org/10.1002/jcc.21759.

(32) Grimme, S.; Antony, J.; Ehrlich, S.; Krieg, H. A Consistent and Accurate Ab Initio Parametrization of Density Functional Dispersion Correction (DFT-D) for the 94 Elements H-Pu. *J. Chem. Phys.* **2010**, *132* (15), 154104. https://doi.org/10.1063/1.3382344.

(33) Henkelman, G.; Uberuaga, B. P.; Jónsson, H. Climbing Image Nudged Elastic Band Method for Finding Saddle Points and Minimum Energy Paths. *J. Chem. Phys.* **2000**, *113* (22), 9901–9904. https://doi.org/10.1063/1.1329672.

(34) Ásgeirsson, V.; Birgisson, B. O.; Bjornsson, R.; Becker, U.; Neese, F.; Riplinger, C.; Jónsson, H. Nudged Elastic Band Method for Molecular Reactions Using Energy-Weighted Springs Combined with Eigenvector Following. *J. Chem. Theory Comput.* **2021**, *17* (8), 4929–4945. https://doi.org/10.1021/acs.jctc.1c00462.

(35) Kozuch, S.; Gruzman, D.; Martin, J. M. L. DSD-BLYP: A General Purpose Double Hybrid Density Functional Including Spin Component Scaling and Dispersion Correction. *J. Phys. Chem. C* **2010**, *114* (48), 20801–20808. https://doi.org/10.1021/jp1070852.

(36) Goerigk, L.; Grimme, S. A Thorough Benchmark of Density Functional Methods for General Main Group Thermochemistry, Kinetics, and Noncovalent Interactions. *Phys. Chem. Chem. Phys.* **2011**, *13* (14), 6670–6688. https://doi.org/10.1039/c0cp02984j.

(37) Klamt, A.; Schüürmann, G. COSMO: A New Approach to Dielectric Screening in Solvents with Explicit Expressions for the Screening Energy and Its Gradient. *J. Chem. Soc. Perkin*

Trans. 2 **1993**, No. 5, 799–805. https://doi.org/10.1039/P29930000799.

(38) Sinnecker, S.; Rajendran, A.; Klamt, A.; Diedenhofen, M.; Neese, F. Calculation of Solvent Shifts on Electronic G-Tensors with the Conductor-like Screening Model (COSMO) and Its Self-Consistent Generalization to Real Solvents (Direct COSMO-RS). *J. Phys. Chem. A* **2006**, *110* (6), 2235–2245. https://doi.org/10.1021/jp056016z.

(39) Kunz, L.; Maier, L.; Tischer, S.; Deutschmann, O. Modeling the Rate of Heterogeneous Reactions. In *Modeling and Simulation of Heterogeneous Catalytic Reactions*; Deutschmann, O., Ed.; Wiley-VCH Verlag GmbH & Co. KGaA: Weinheim, Germany, 2011; pp 113–148. https://doi.org/10.1002/9783527639878.ch4.

(40) Balcells, D.; Nova, A.; Clot, E.; Gnanamgari, D.; Crabtree, R. H.; Eisenstein, O. Mechanism of Homogeneous Iridium-Catalyzed Alkylation of Amines with Alcohols from a DFT Study. *Organometallics* **2008**, *27* (11), 2529–2535. https://doi.org/10.1021/om800134d.

(41) Zhao, J.; Hesslink, H.; Hartwig, J. F. Mechanism of β-Hydrogen Elimination from Square Planar Iridium(I) Alkoxide Complexes with Labile Dative Ligands. *J. Am. Chem. Soc.* **2001**, *123* (30), 7220–7227. https://doi.org/10.1021/ja010417k.

(42) Glueck, D. S.; Winslow, L. J. N.; Bergman, R. G. Iridium Alkoxide and Amide Hydride Complexes. Synthesis, Reactivity, and the Mechanism of O-H and N-H Reductive Elimination. *Organometallics* **1991**, *10* (5), 1462–1479. https://doi.org/10.1021/om00051a044.

(43) Murdoch, J. R. What Is the Rate-Limiting Step of a Multistep Reaction? *J. Chem. Educ.* **1981**, *58* (1), 32. https://doi.org/10.1021/ed058p32.

(44) Shvo, Y.; Czarkie, D.; Rahamim, Y.; Chodosh, D. F. A New Group of Ruthenium Complexes: Structure and Catalysis. *J. Am. Chem. Soc.* **1986**, *108* (23), 7400–7402. https://doi.org/10.1021/ja00283a041.

(45) Comas-Vives, A.; Ujaque, G.; Lledós, A. Mechanistic Evaluation of Metal-Catalyzed Hydrogen-Transfer Processes: The Shvo Catalyst as an Example of Computational Unravelling. *J. Mol. Struct. THEOCHEM* **2009**, *903* (1–3), 123–132. https://doi.org/10.1016/j.theochem.2008.11.043.

(46) Chen, Y.; Liu, S.; Lei, M. Nature of Asynchronous Hydrogen Transfer in Ketone Hydrogenation Catalyzed by Ru Complex. *J. Phys. Chem. C* **2008**, *112* (35), 13524–13527. https://doi.org/10.1021/jp8003807.

(47) Mitrichev, I. I. *mech_optimiz: software that assists in construction of microkinetic mechanisms of heterogeneous catalytic reactions*. http://imitrichev.github.io/mech_optimiz/main.html (accessed 2025-02-07).

(48) Mitrichev, I. I.; Zhensa, A. V.; Kol'tsova, E. M. Thermodynamic Criteria for Estimating the Kinetic Parameters of Catalytic Reactions. *Russ. J. Phys. Chem. A* **2017**, *91* (1), 44–51. https://doi.org/10.1134/S0036024417010186.

(49) Goerigk, L.; Hansen, A.; Bauer, C.; Ehrlich, S.; Najibi, A.; Grimme, S. A Look at the Density Functional Theory Zoo with the Advanced GMTKN55 Database for General Main Group Thermochemistry, Kinetics and Noncovalent Interactions. *Phys. Chem. Chem. Phys.* **2017**, *19* (48), 32184–32215. https://doi.org/10.1039/c7cp04913g.

(50) Campbell, C. T. The Degree of Rate Control: A Powerful Tool for Catalysis Research. *ACS*

Catal. **2017**, *7* (4), 2770–2779. https://doi.org/10.1021/acscatal.7b00115.

(51) Stegelmann, C.; Andreasen, A.; Campbell, C. T. Degree of Rate Control: How Much the Energies of Intermediates and Transition States Control Rates. *J. Am. Chem. Soc.* **2009**, *131* (23), 8077–8082. https://doi.org/10.1021/ja9000097.

(52) Cortright, R. D.; Dumesic, J. A. Kinetics of Heterogeneous Catalytic Reactions: Analysis of Reaction Schemes. *Adv. Catal.* **2001**, *46*, 161–264. https://doi.org/10.1016/S0360-0564(02)46023-3.

(53) Hall, A. M. R.; Dong, P.; Codina, A.; Lowe, J. P.; Hintermair, U. Kinetics of Asymmetric Transfer Hydrogenation, Catalyst Deactivation, and Inhibition with Noyori Complexes As Revealed by Real-Time High-Resolution FlowNMR Spectroscopy. *ACS Catal.* **2019**, *9* (3), 2079–2090. https://doi.org/10.1021/acscatal.8b03530.

(54) Clapham, S. E.; Hadzovic, A.; Morris, R. H. Mechanisms of the H2-Hydrogenation and Transfer Hydrogenation of Polar Bonds Catalyzed by Ruthenium Hydride Complexes. *Coord. Chem. Rev.* **2004**, *248* (21–24), 2201–2237. https://doi.org/10.1016/j.ccr.2004.04.007.

TOC graphic

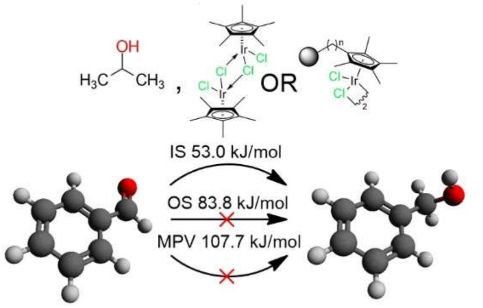
OH
H3C
CH3
Ir
Cl
OR
n
2
IS 53.0 kJ/mol
OS 83.8 kJ/mol
MPV 107.7 kJ/mol